Supplement of Ocean Sci., 20, 1611–1630, 2024
https://doi.org/10.5194/os-20-1611-2024-supplement

Ocean Science Open Access EGU

Supplement of

Transient Attracting Profiles in the Great Pacific Garbage Patch

Luca Kunz et al.

Correspondence to: Luca Kunz (luca.kunz@orac.earth)

S1 Supplementary figures

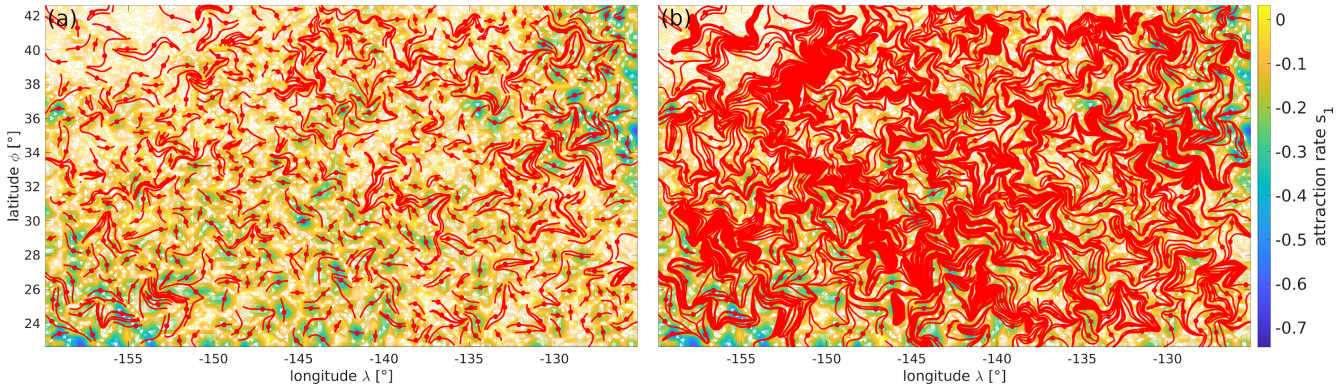

Figure S1. TRAPs with different lengths. (a) TRAPs are computed with a maximal arclength of 100 degrees and a cutoff at 30 % of core attraction strength. (b) TRAPs are computed for the same snapshot as in (a) but with a maximal arclength of 100 degrees and no cutoff. Note that the colourmap indicating the $s_1(\boldsymbol{x}, t_0)$ strain field at snapshot time t_0 is inverse to the one used in Fig. 2 of the article. We created this particular image using the default plotting utility provided by Serra (2020).

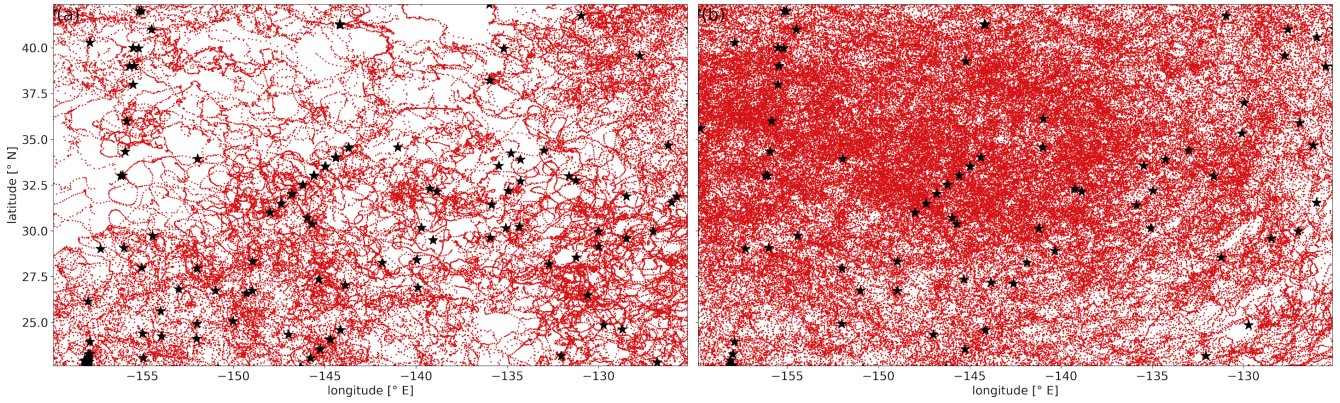

Figure S2. Drifter positions within the study domain and period 2000-2019. (a) Circle markers indicate 24-hourly drifter positions at UTC midnight for drogued drifters from the Global Drifter Program (Lumpkin and Centurioni, 2019). Black stars indicate the deployment sites of the respective drifters. (b) as (a) but for undrogued drifters.

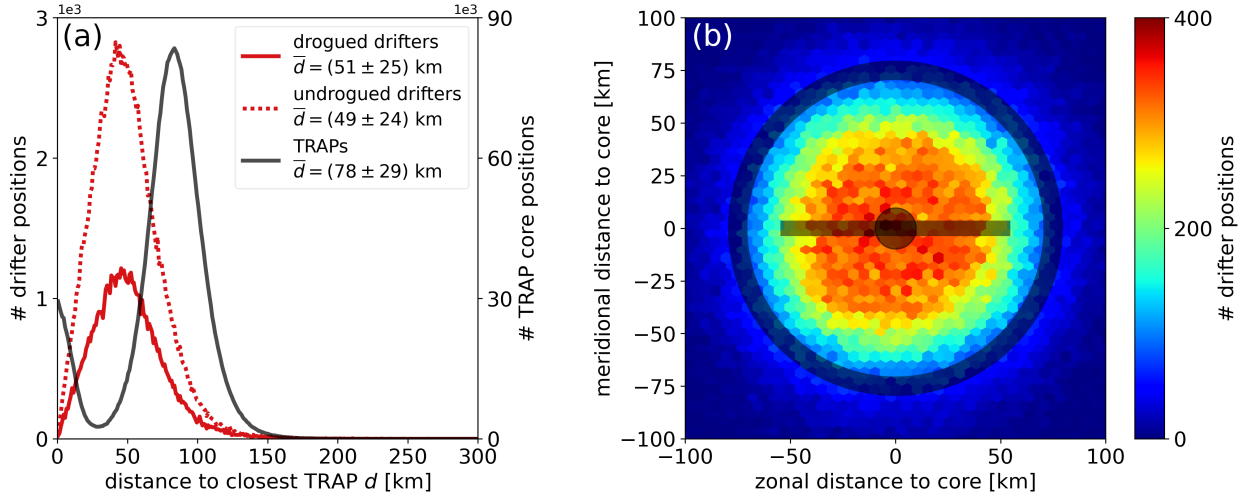

Figure S3. Drifter distances to TRAPs. (a) Distribution of distances between drifter positions and their closest TRAP core (red lines), as well as between TRAP core positions and their closest, neighbouring TRAP core (black line). (b) Spatial histogram of drifter position counts around their closest TRAP. Similar to Fig. 10 within the article, drifter positions are rotated towards the zonal axis and counted within hexagonal bins.

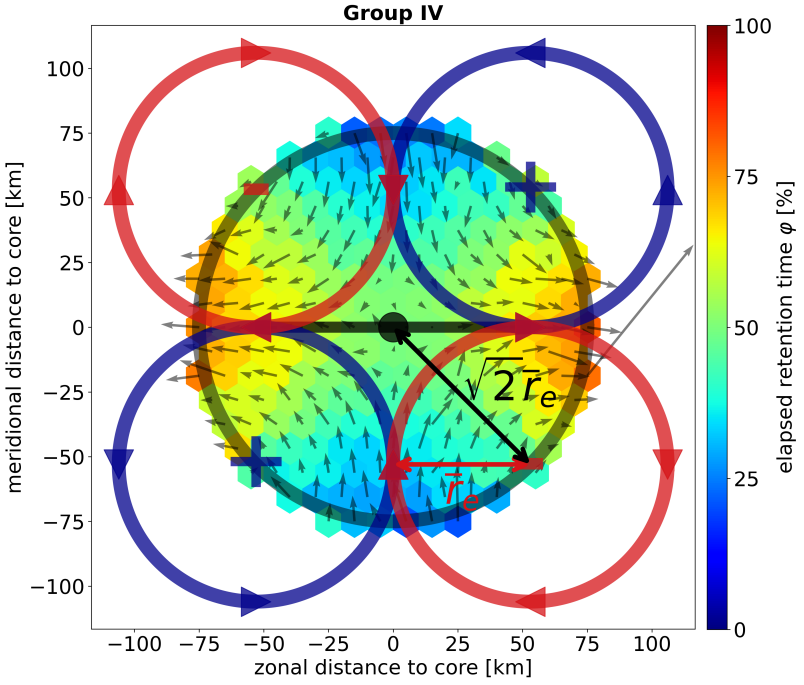

Figure S4. Drifter motion around TRAPs and eddies. We embed Fig. 10d of the article in a scheme of four idealised mesoscale eddies. Blue and red circles represent cyclonic and anticyclonic mesoscale eddies, respectively, with a radius equal to the mean radius $\overline{r}_e \approx 53$ km that we find for mesoscale eddies in our domain, using eddy detections from AVISO+ et al. (2022). $\overline{r}_e$ determines the search radius $r_s = \sqrt{2}\overline{r}_e$ of our drifter-TRAP pair algorithm. A transparent TRAP in the middle represents a generic profile, the black circle draws the limits of the drifter search zone around it. The rotation of the idealised eddies aligns with the hyperbolic drifter motion we observe around mature TRAPs.

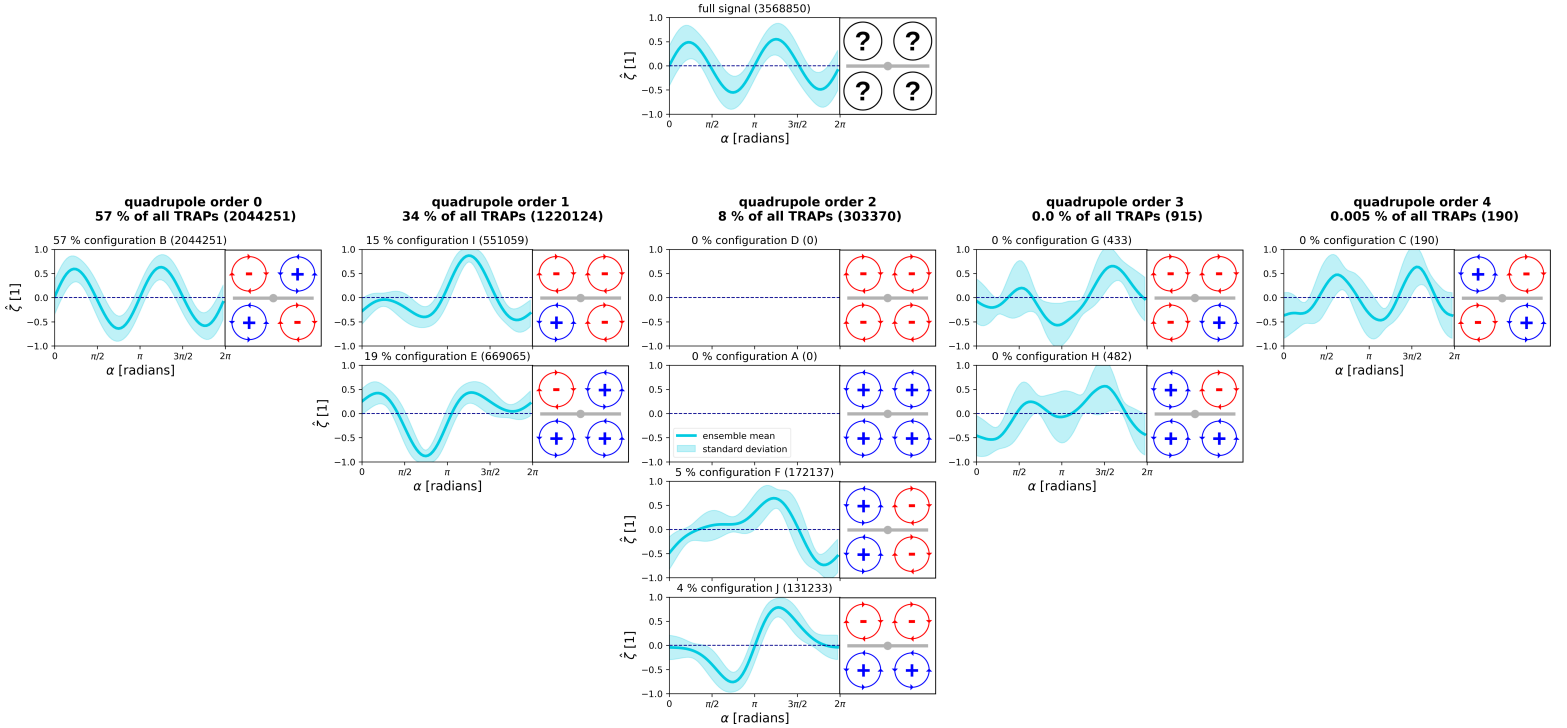

Figure S5. Vorticity patterns around TRAPs. We remove a constant average background vorticity from each of the 3,568,850 vorticity curves $\zeta(\alpha)$ and filter the ensemble for combinations of four vortices that are unique under rotations of 180° around a TRAP core. We derive 10 unique vorticity patterns, and for every pattern, we present the mean and standard deviation of the associated normalised vorticity curves $\hat{\zeta}(\alpha)$ as blue lines and shaded bands, respectively. The normalisation again only serves for visualisation purposes. We illustrate each configuration with cyclonic (blue) and anticyclonic (red) vortices around a grey TRAP. Titles indicate the count of each pattern and its share in the overall signal. The patterns are grouped by their quadrupole order q with q increasing from left to right.

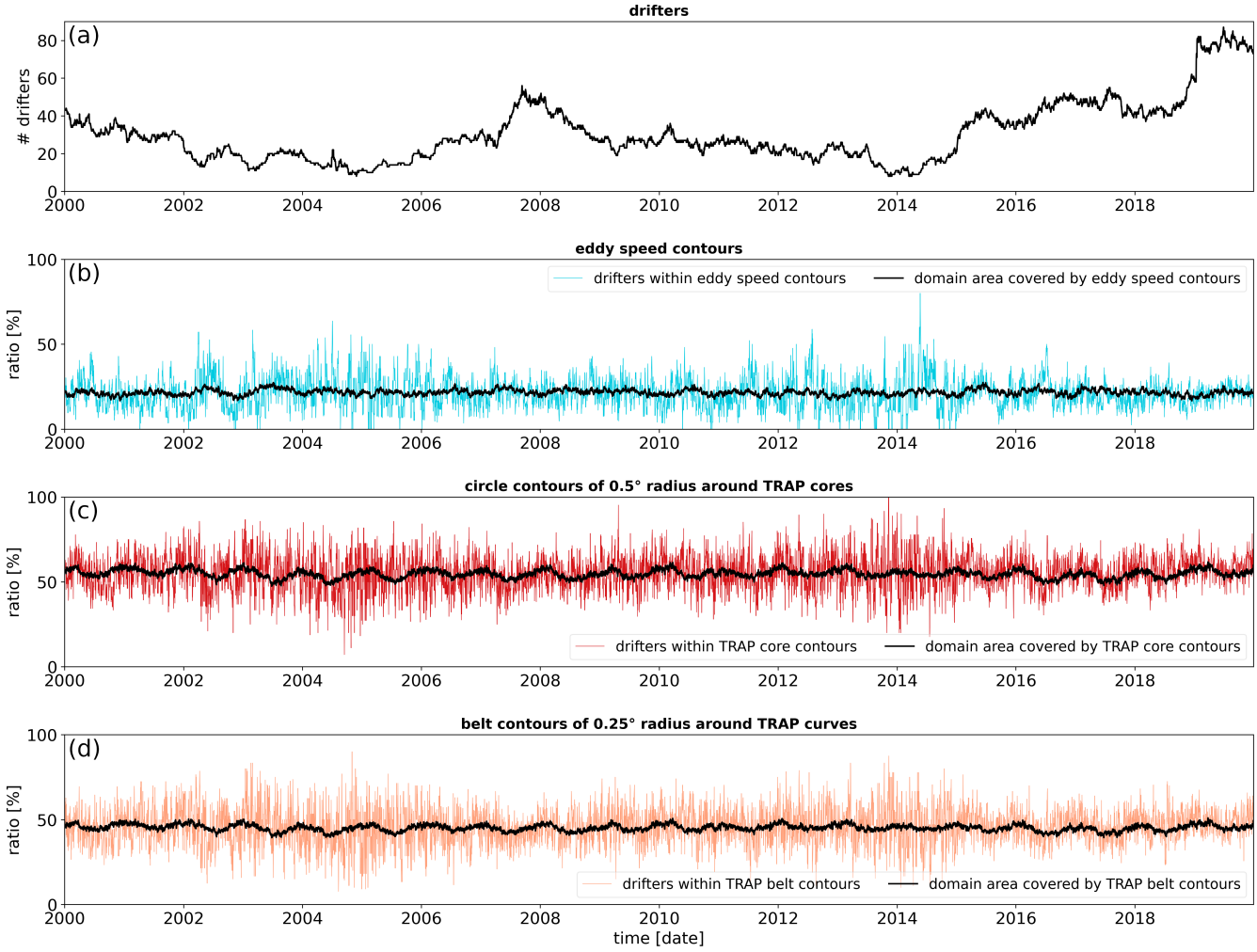

Figure S6. Time series of surface area enclosed by, and drifter positions detected within TRAP and eddy contours. (a) Time series of the daily number of drifter positions within the study domain. (b) The black line indicates the proportion of domain area covered by daily eddy speed contours. The coloured line represents the ratio of daily drifter positions within these eddy contours. (c) and (d) as (b) but for contours around TRAP cores and TRAP curves, respectively. Mesoscale eddies as detected by AVISO+ et al. (2022).

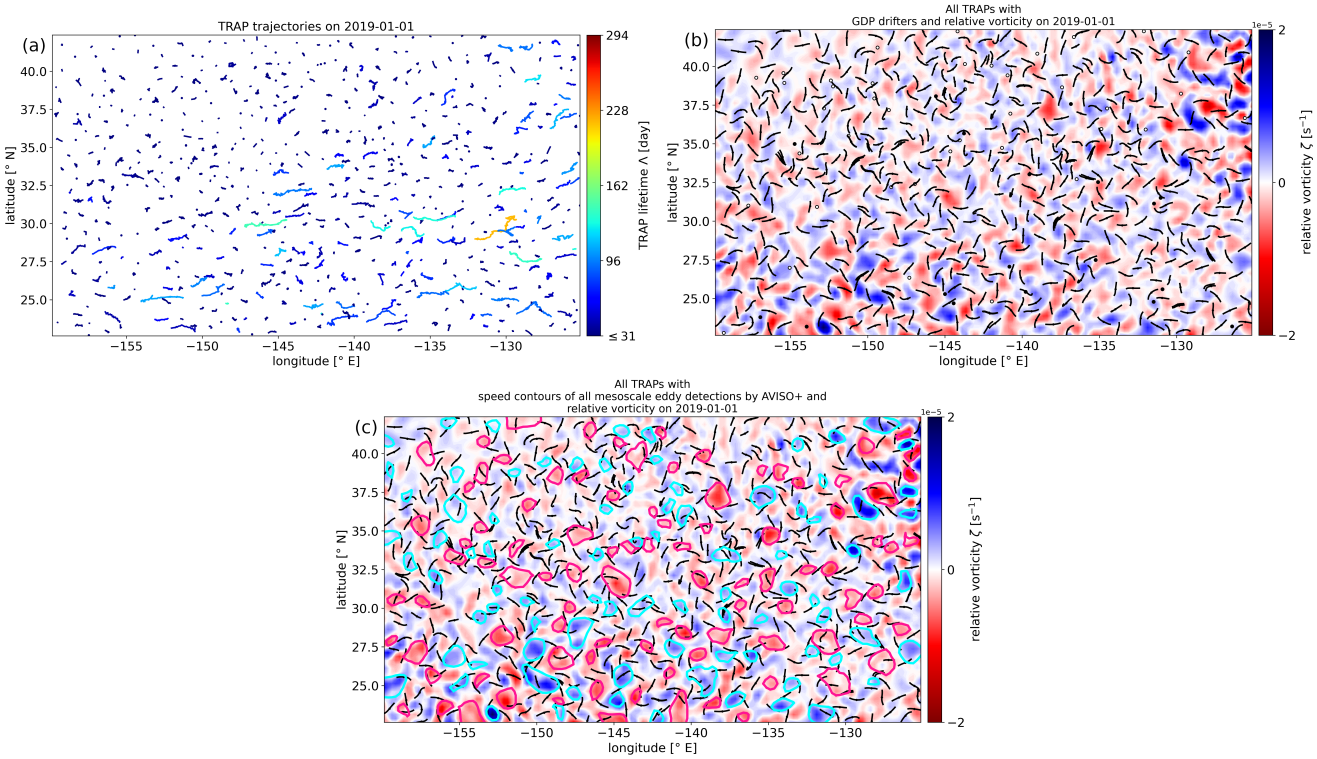

Figure S7. Information about supplementary videos. (a) Coloured lines represent the trajectories of propagating TRAPs, which we derive with our tracking algorithm. Colours indicate the estimated total lifetime of a TRAP, ephemeral TRAPs appear as flickering points in the respective Supplementary Video S1. (b) Black lines indicate TRAPs upon a colourmap of the relative vorticity field $\zeta(\boldsymbol{x}, t_0)$ at snapshot time t_0. Filled and empty black circles represent the 24-hourly positions of drogued and undrogued drifters, respectively, provided by Lumpkin and Centurioni (2019). Video S2 then shows the simultaneous motion of TRAPs, drifters and the evolution of the relative vorticity field. (c) as (b) but for detections of mesoscale eddies instead of drifter positions. Video S3 animates the simultaneous propagation of TRAPs and eddies. Blue lines indicate the speed contour of cyclonic, and pink lines the speed contour of anticyclonic eddy detections by AVISO+ et al. (2022).

S2 Choice of ϵ

We define the search area around a TRAP to look for future detections by a box reaching $\pm\epsilon$ in zonal and meridional direction around the position of the current TRAP core. We have tested the tracking algorithm for different values of ϵ and find that the distribution of TRAP lifetimes Λ broadens with increasing ϵ until it remains practically constant for $\epsilon \geq 0.75°$. The longest TRAP lifetime Λ_{max} likewise plateaus for $\epsilon \geq 0.75°$. Table S1 lists the tested values of ϵ together with the respective value of Λ_{max}. The broadening of the lifetime distribution from $\epsilon = 0.1°$ to $\epsilon = 0.75°$ occurs because small values of ϵ will lead to underestimated while large values of ϵ to overestimated TRAP trajectory lengths. In the first case, the search box is too small to capture the future position of a TRAP, whereas in the last case, the algorithm creates "jumps" from a current to an unrealistically far future TRAP detection. To choose a sensible ϵ-value from this range, we can derive the highest possible absolute TRAP propagation speed $c_{max}(\epsilon)$ in each realisation and compare it to propagation speeds of mesoscale eddies, as given in Abernathey and Haller (2018) or Chelton et al. (2011), because we expect a relation between these mesoscale flow features.

ϵ defines the maximal distance which can be tracked between a current and a future TRAP position. This distance limit ranges between ϵ in purely zonal or meridional direction and $\sqrt{2}\epsilon$ in purely northwest, southwest, southeast or northeast direction, i.e. into each corner of the box. The upper threshold for the absolute TRAP propagation speed $c_{max}(\epsilon)$ consequently depends on direction and ranges between $c^{+}_{max}(\epsilon)$ in purely zonal or meridional direction and $c^{\times}_{max}(\epsilon)$ in purely northeast, northwest, southwest or southeast direction. Practically, the algorithm allows higher propagation speeds towards intercardinal directions. The limits of this range can be approximated as follows:

$$c^{+}_{max}(\epsilon) \approx \frac{111120\ \mathrm{m}}{1\ \text{degree arclength}} \cdot \frac{\epsilon}{86400\ \mathrm{s}}$$

$$c^{\times}_{max}(\epsilon) = \sqrt{2} \cdot c^{+}_{max}(\epsilon)$$

A future version of the algorithm should use a search circle to remove this sensitivity on direction. Table S1 presents the values of c^{+}_{max} and $c^{\times}_{max}$ for each test run. Propagation speeds of mesoscale eddies typically range below $0.2\ \mathrm{m\ s^{-1}}$ and even less for the latitudes that we study (Abernathey and Haller, 2018; Chelton et al., 2011). Therefore it seemed reasonable to discard test runs with $\epsilon \geq 0.5°$ because they certainly include TRAPs with propagation speeds above $0.32\ \mathrm{m\ s^{-1}}$ which is revealed by the increase of Λ_{max} when switching from $\epsilon = 0.25°$ to $\epsilon = 0.5°$. On the other hand, $\epsilon = 0.1°$ could be too restrictive on TRAP propagation speeds because mesoscale features might, even if rarely, move with speeds above $0.13\ \mathrm{m\ s^{-1}}$. Moreover, $\epsilon = 0.1°$ is below the technical resolution of our velocity data. For these reasons, we chose $\epsilon = 0.25°$ for the analysis.

Table S1. Values of the search box parameter ϵ for which the tracking algorithm has been tested, together with the highest TRAP lifetime measured Λ_{max} and the upper thresholds for absolute TRAP propagation speed $c^{+}_{max}(\epsilon)$ in purely zonal or meridional direction and $c^{\times}_{max}(\epsilon)$ in purely northeast, northwest, southwest or southeast direction.

ϵ [degree arclength]	0.10	0.25	0.50	0.75	1.00	1.25	1.50
Λ_{max} [day]	197	294	302	321	321	321	321
c^{+}_{max} [m s^{-1}]	0.13	0.32	0.64	0.97	1.29	1.60	1.93
$c^{\times}_{max}$ [m s^{-1}]	0.18	0.46	0.91	1.36	1.82	2.27	2.73

After the tracking procedure, we computed the zonal and meridional propagation speed of individual TRAP detections, which allows us to compare the distribution of absolute TRAP translation speeds c with the estimated thresholds c^{+}_{max} and $c^{\times}_{max}$ from Table S1 and to evaluate our choice of $\epsilon = 0.25°$. We further measured the surface geostrophic + Ekman current velocity at the position of every TRAP core, which provides an additional distribution of flow velocities around these features. In Fig. S7, we show these two distributions of absolute TRAP and surface water velocities.

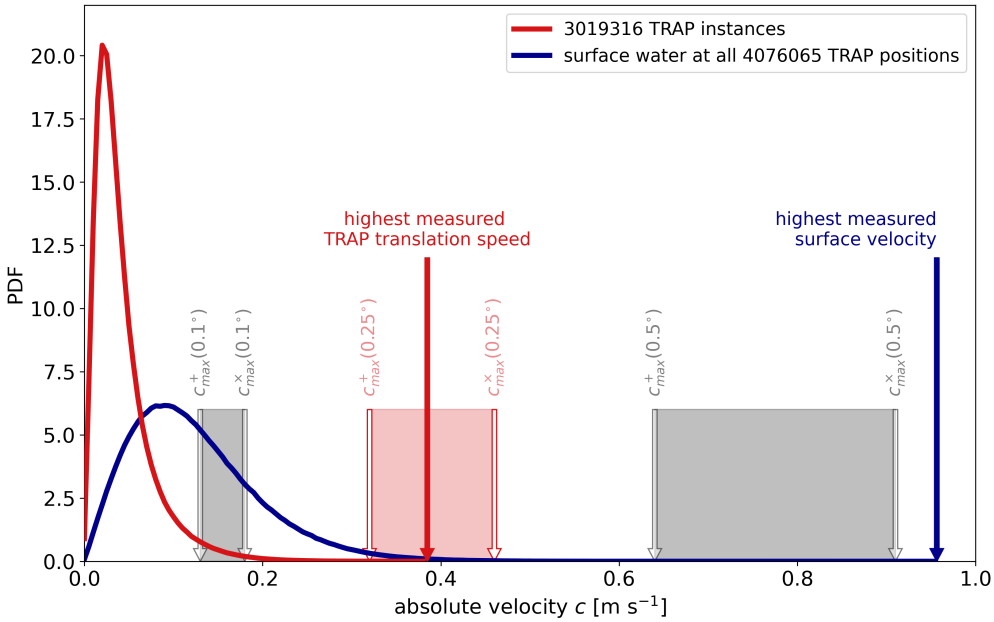

Figure S8. Distributions of absolute TRAP and surface water velocities. The red line illustrates the distribution of all measured absolute TRAP translation speeds c. The blue line presents the distribution of absolute surface geostrophic + Ekmann current velocities measured at *all* TRAP positions. Filled arrows indicate the maximum value of each distribution, empty arrows the upper thresholds $c^{+}_{max}(\epsilon)$ and $c^{\times}_{max}(\epsilon)$ of absolute TRAP propagation speed, displayed for three values of the search box parameter ϵ. The shaded bands illustrate the range between these upper thresholds, which results from the dependence of $c_{max}(\epsilon)$ on direction due to the geometry of the search box.

First, we see a clear difference between both distributions, indicating that TRAPs are not advected by the flow. TRAP propagation speeds are generally smaller than geostrophic + Ekman currents. Next, we see that a choice of $\epsilon = 0.1°$ would have caused an underestimation of TRAP trajectory lengths since the respective limits of $c^{+}_{max}(0.1°)$ and $c^{\times}_{max}(0.1°)$ would cut off the smooth tail of the distribution of TRAP propagation speeds. This is different for the choice of $\epsilon = 0.25°$ where most of the tail is preserved by $c^{+}_{max}(0.25°)$ and the distribution ends well before $c^{\times}_{max}(0.25°)$. It suggests that the search box is large enough to capture the majority of TRAP propagation speeds, i.e. future TRAP positions, in any direction. And it is small enough to prevent "jumps" to unrealistically far future TRAP detections, in intercardinal directions, that would artificially extend the distribution up to the limit of $c^{\times}_{max}(0.25°)$. Since the highest measured TRAP translation speed lies clearly within the range between $c^{+}_{max}(0.25°)$ and $c^{\times}_{max}(0.25°)$, we expect the optimal value of ϵ within this range. Future studies could fine-tune this parameter using a search circle instead of a box. Optimising ϵ for TRAPs at different scales would be another valuable contribution since it makes the tracking algorithm applicable to different velocity sources.

S3 Spatial analysis of TRAP trajectories

In Section 2 of the Supplementary Material and the documentation of our tracking algorithm (Kunz, 2024), we define the search area around a TRAP to look for future detections by a box reaching $\pm\epsilon$ in zonal and meridional direction around the position of the current TRAP core. In Section 2, we motivate our choice of $\epsilon = 0.25°$ and we use this parameter in Kunz (2024) to define a smaller ϵ-domain with the new boundaries displaced by ϵ from the original domain boundaries. The boundaries of the ϵ-domain are exclusive.

When a TRAP core is located outside the ϵ-domain, its past/future position within the search box may be on or beyond the boundaries of the original study domain - but we do not detect TRAPs there. As a consequence, TRAP trajectories that reach beyond the ϵ-domain have the potential to be shortened because they might originate from outside the domain or continue there. Their lifetime would then be underestimated. But lifetimes can also be overestimated beyond the ϵ-domain due to a wrong association of two close trajectories for which additional data is hidden behind the boundaries of the study domain. The algorithm corrects to some extent for the second case, see *bias circles* in Kunz (2024), while it is agnostic to the first case. Because the second case presupposes the first one, we expect that lifetimes are generally underestimated for detections beyond the ϵ-domain.

A similar boundary error may occur at the temporal limits of our dataset. TRAP trajectories that start on the first or end on the last day of our record might have existed before or might continue to exist after the study period, respectively.

To estimate the bias that might result from these boundary effects, we filter the TRAPs record for trajectories that reach outside the ϵ-domain or occur on the first or the last snapshot of our record. We find that 5.4 % of all TRAP trajectories fulfil one of these conditions and are therefore susceptible to a spurious lifetime estimation (with 5.2 percentage points being attributed to the spatial limits only). We flag these trajectories as potential bias and define four groups of trajectories:

1. the *biased* dataset, i.e. the original TRAPs record
2. the *bias* subset of trajectories with potentially spurious lifetime estimation
3. the *debiased* subset, which only consists of trajectories that stay within the tempo-spatial limits of the experiment, i.e. the biased set excluding the bias set
4. the *corrected* dataset with lifetimes increased by 13 days for all trajectories that are part of the bias subset, 13 days is 1 standard deviation of the lifetime distribution within the debiased set

In Fig. S8, we present the distribution of TRAP lifetime Λ within each of these groups. It illustrates that the bias potentially introduced by the tempo-spatial limits of the experiment, i.e. trajectories entering or leaving the domain and period, is negligible since the biased and debiased lifetime distributions in panel (a) as well as the biased and corrected distributions in panel (b) almost perfectly coincide. In panel (b), we try to compensate for lifetime underestimation by increasing spurious lifetimes by 1 standard deviation of the debiased distribution.

In Table S2, we compare a few statistics for the biased, the debiased and the corrected datasets. The subtle differences between the subsets confirm that these boundary effects are negligible and that the 5.4 % potentially spurious lifetime estimations do not affect the main findings of our paper. We note that our approach here is conservative and will produce false positives, which require an individual examination. Future studies might, however, try to further reduce the impact of these boundary effects by choosing a larger domain.

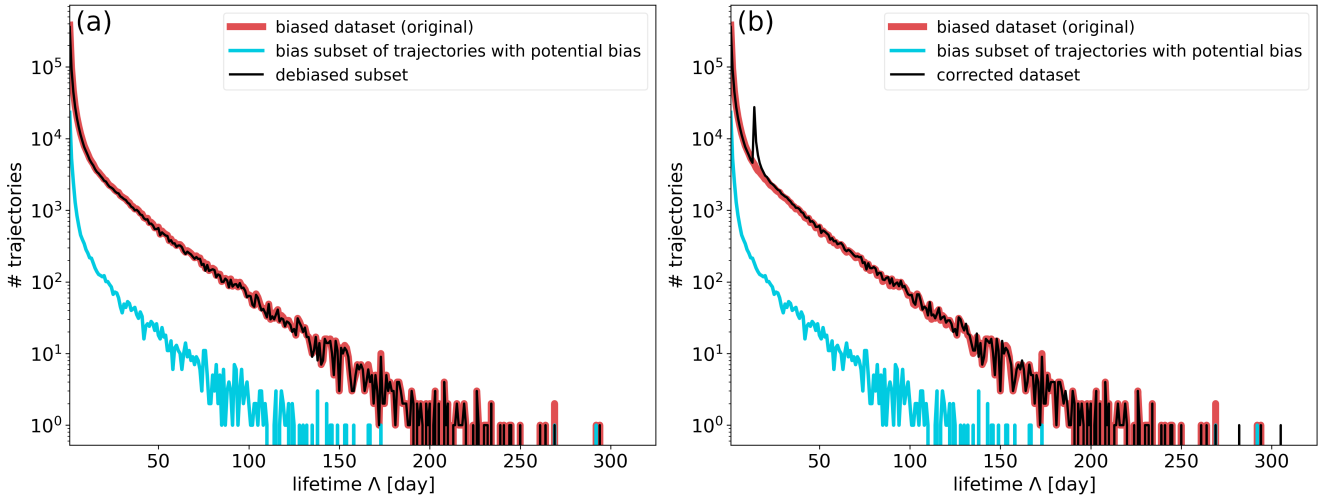

Figure S9. Distribution of TRAP lifetime Λ for different subsets of the TRAPs record. (a) The red line indicates the distribution within the *biased* dataset, i.e. the original TRAPs record as shown in Fig. 5 of the article, the blue line represents the distribution of the *bias* subset, and the black line indicates the *debiased* subset. (b) as (a) but with the black line indicating the distribution for the *corrected* dataset.

Table S2. Comparison between TRAP lifetime statistics from the biased (original), the debiased and the corrected datasets. Trajectories that might enter or leave the study domain or period represent the potential bias. Mean values are given together with 1 standard deviation σ.

Section in article	metric	biased dataset	debiased dataset	corrected dataset
3.2	average TRAP lifetime $\overline{\Lambda}$	(5.66 ± 12.38) days	(5.74 ± 12.48) days	(6.36 ± 12.65) days
3.2	share of long-living TRAP trajectories with $\Lambda > 30$ days	4.3 %	4.4 %	4.5 %
3.2	share of TRAP instances associated with long-living TRAP trajectories with $\Lambda > 30$ days	40.5 %	40.8 %	41.1 %
3.1	mean attraction strength $\overline{s}_1$ of instances associated with long-living TRAPs with $\Lambda > 30$ days	(-0.283 ± 0.111) s^{-1}	(-0.281 ± 0.108) s^{-1}	(-0.283 ± 0.111) s^{-1}
3.1	mean attraction strength $\overline{s}_1$ of instances associated with "short"-living TRAPs with $\Lambda \leq 30$ days	(-0.198 ± 0.087) s^{-1}	(-0.197 ± 0.084) s^{-1}	(-0.197 ± 0.085) s^{-1}

References

Abernathey, R. and Haller, G.: Transport by Lagrangian Vortices in the Eastern Pacific, Journal of Physical Oceanography, 48, 667–685, https://doi.org/10.1175/JPO-D-17-0102.1, 2018.

AVISO+, CNES, SSALTO/DUACS, and IMEDEA: The altimetric Mesoscale Eddy Trajectories Atlas 3.2 Delayed-Time (META3.2 DT) Allsat Version, AVISO+ [dataset], https://doi.org/10.24400/527896/a01-2022.005.220209, 2022.

Chelton, D. B., Schlax, M. G., and Samelson, R. M.: Global observations of nonlinear mesoscale eddies, Progress in Oceanography, 91, 167–216, https://doi.org/10.1016/j.pocean.2011.01.002, 2011.

Kunz, L.: Track and analyse Transient Attracting Profiles in the Great Pacific Garbage Patch, Zenodo [code], https://doi.org/10.5281/zenodo.12761097, 2024.

Lumpkin, R. and Centurioni, L.: Global Drifter Program quality-controlled 6-hour interpolated data from ocean surface drifting buoys, NOAA National Centers for Environmental Information [dataset], https://doi.org/10.25921/7ntx-z961, 2019.

Serra, M.: Compute Transient Attracting Profiles (TRAPs), GitHub [code], https://github.com/MattiaSerra/TRAPs, 2020.